Material Properties of Lipid Microdomains: Force-Volume Imaging Study of the Effect of Cholesterol on Lipid Microdomain Rigidity

Hongjie An,[†] Matthew R. Nussio,[†] Mickey G. Huson,[‡] Nicolas H. Voelcker,[†*] and Joseph G. Shapter[†*]
[†]School of Chemical and Physical Sciences, Flinders University, Adelaide, Australia; and [‡]Materials Science and Engineering, Commonwealth Scientific and Industrial Research Organisation, Geelong, Australia

ABSTRACT The effect of cholesterol (CHOL) on the material properties of supported lipid bilayers composed of lipid mixtures that mimic the composition of lipid microdomains was studied by force-volume (FV) imaging under near-physiological conditions. These studies were carried out with lipid mixtures of dioleoylphosphatidylcholine, dioleoylphosphatidylserine, and sphingomyelin. FV imaging enabled simultaneous topology and force measurements of sphingomyelin-rich domains (higher domain (HD)) and phospholipid-rich domains (lower domain (LD)), which allowed quantitative measurement of the force needed to puncture the lipid bilayer with or without CHOL. The force required to penetrate the various domains of the bilayer was probed using high- and low-ionic-strength buffers as a function of increasing amounts of CHOL in the bilayer. The progressive addition of CHOL also led to a decreasing height difference between HD and LD. FV imaging further demonstrated a lack of adhesion between the atomic force microscope tip and the HD or LD at loads below the breakthrough force. These results can lead to a better understanding of the role that CHOL plays in the mechanical properties of cellular membranes in modulating membrane rigidity, which has important implications for cellular mechanotransduction.

INTRODUCTION

Membrane rafts have been defined as ''small (10–200 nm), heterogeneous, highly dynamic, sterol- and sphingolipid-enriched domains that compartmentalize cellular processes'' (1). These microdomains, which are recognized as detergent-resistant membranes, are postulated to be biologically important because of their physical and chemical properties (2,3). According to the raft hypothesis, sphingolipids and cholesterol (CHOL) preferentially pack into laterally organized regions in which proteins can be selectively included or excluded (4–6). In humans, CHOL accounts for as much as 50 mol % of lipid composition (7) and plays an important role in physiological functions such as maintaining membrane thickness and fluidity (8), limiting ion leakage (9), ensuring signal transduction (10,11), trafficking membrane proteins (12–14), mediating certain neurodegenerative disorders (15), and causing infertility (16). CHOL has also been shown to play a key role in mechanotransduction processes in endothelial cells and differential activation of extracellular signal-regulated kinase due to shear stress or hydrostatic pressure (17,18).

Lipid-lipid interactions are fundamentally important for the emergence of lateral membrane heterogeneity. Close packing with the saturated acyl chains of sphingolipids, as opposed to looser packing in unsaturated phospholipids, probably leads to phase separation. With high levels of CHOL, the subdomains exist as liquid-ordered regions and exhibit less fluid properties (19). It is believed that lateral heterogeneity in defiance of the membrane's fluid nature influences protein function directly by modulating membrane properties (20). However, there is a disconnect between lipid microdomains derived from biochemical and biophysical assays and localized measurements, since the physical tools used to study lipid microdomains are still being developed. To address the lack of understanding of membrane organization and its mechanical rigidity, investigators have attempted to characterize (with nanometer resolution) lipid membrane spatial organization in the presence of CHOL (21–23).

Supported lipid bilayers (SLBs), which are formed by spreading vesicles from solution onto suitable substrates, have become popular models of cellular membranes for fundamental and applied biophysical studies of membrane structure (24,25), drug interactions (26–29), and transmembrane protein structure (30,31). SLB membranes constitute an attractive reductive system for studying membrane physiological processes in proteins and other membrane-active biomolecules in a biomimetic environment (32–35).

Chemically identifying and quantifying the lateral composition of multicomponent bilayers is a difficult task. The possibility of a different lipid composition in the two leaflets of the bilayer exacerbates the problem, and techniques to chemically analyze membrane components in both leaflets are unavailable (36). A form of high-resolution secondary ion mass spectrometry, termed NanoSIMS, has revealed lipid distribution within a phase-separated membrane with a lateral resolution of ~100 nm (22). However, NanoSIMS is performed in a vacuum and requires freeze-drying before analysis using isotope labels. This environment is not reflective of physiological conditions, and dynamic variations in lipid distribution are not accessible by NanoSIMS. Fluorescence microscopy and fluorescence correlation spectroscopy

Submitted August 4, 2009, and accepted for publication April 30, 2010.

*Correspondence: joe.shapter@flinders.edu.au or nico.voelcker@flinders.edu.au

Editor: Peter Hinterdorfer.

0006-3495/10/08/0834/11 $2.00

doi: 10.1016/j.bpj.2010.04.072

have been employed to visualize distinct lipid phases and lateral heterogeneities within membranes using dye-labeled lipids or polarity-sensitive probes (37–42). However, the lateral resolution of such fluorescence-based techniques is diffraction-limited, and the required fluorescently labeled lipids have been reported to perturb membrane organization (43–45).

High-resolution atomic force microscopy (AFM) has been applied to study biological membranes (21,24,26), and lateral and chemical force microscopy has been used to investigate the mechanical properties of phospholipid bilayer domains and phases (46). Employing lateral force microscopy to measure mechanical property variations associated with the chemical components within these bilayers is challenging because such measurements are prone to cause surface defects due to the scanning tip perturbing or even puncturing the soft membrane surface (46).

With the use of pulsed force mode scanning force microscopy (PFM-SFM), contrasts in adhesion for ternary mixtures of SLBs have been achieved (47). Force spectra reveal a higher adhesion for dioleoylphosphatidylcholine (DOPC)-rich phases, in contrast to domains rich in sphingomyelin (SM) and CHOL. Contrast in adhesion is a result of deeper tip penetration into the DOPC liquid phase. The capacity of the tip to penetrate the membrane is related to the maximum force applied, which is known as the trigger threshold. This technique can provide high-spatial-resolution images of membranes; however, it does not provide postprocessing quantitative force curves, because only the stiffness (slope) and adhesion (pull-off force) values from each point are stored.

In the recently developed digital pulsed force mode (DPFM), force curves at each point can be stored and analyzed. However, the resolution of these curves is very low. The force applied to the surface in these pulsed modes is difficult to control and hence surface damage is a possibility (48). This is a severe limitation for soft samples such as SLBs because they are very easy to penetrate, and disruption of the layer will certainly yield incorrect results for both topography and force. Additionally, such penetration will likely destroy the layer and contaminate the AFM probes.

These difficulties can be overcome by a technique known as force-volume (FV) imaging, which measures high-resolution force curves in such a way that topology and interaction forces are measured simultaneously. This technique has been available for some time and has been used to examine polymer properties (49,50) and produce elasticity maps of heterogeneous materials such as biominerals (51), carbon nanotubes (52), polymer composites (50,53,54), and living cells (55–57). FV rasters the AFM tip over the surface to measure forces as a function of position, creating a force density map that is directly correlated to topography. This approach is slower than some recent techniques, but has the twofold advantage of allowing very fine tuning of the maximum (or threshold) force applied and more precise measurement of force curves. This ensures that in soft samples, the proper topography of undisturbed layers is measured with force curves corresponding to interactions between the tip and intact bilayer.

Recent work have reported the nanoscale mapping of bilayer forces (57–62). It is difficult to probe the force behavior of SLBs on the nanometer scale because of position drift during imaging and the conformational and translational variation in bilayers. In-fluid AFM in FV mode can overcome these difficulties. Early pioneering work demonstrated the wealth of information available from such studies (58,59). Additionally, it is possible to examine the mechanics of lipid rafts when CHOL is incorporated. Herein, we present an analysis of model lipid membranes using FV imaging. We obtained topographical information while collecting force curves at each point for multicomponent lipid raft membranes with or without CHOL at a lateral resolution of 20 nm.

MATERIALS AND METHODS

SLBs were prepared as described previously (34) and briefly summarized here. Further details are provided in the Supporting Material (this information is available free of charge at http://www.cell.com/biophysj/). Lipids and CHOL (from Avanti Polar Lipids, Alabaster, AL) in appropriate ratios were dissolved in chloroform to form a bilayer on the vessel walls. After the solvent was removed, they were redissolved in HEPS buffer to yield vesicles of the appropriate composition. After a 12 h incubation, the lipids were extruded to obtain 100 nm diameter vesicles, which were then deposited onto freshly cleaved mica.

Visualization and force measurements of the SLBs were performed using a commercial atomic force microscope (Nanoscope IV; Digital Instruments/Veeco, Santa Barbara, CA) equipped with a J scanner. A quartz fluid cell was used without the o-ring. The samples were imaged using unmodified triangular Si_3N_4 cantilevers (OTR8; Digital Instruments) with a nominal spring constant of 0.15 N m^{-1} operating at a frequency of 7–9 kHz in tapping mode. The same cantilevers were also operated in contact mode to perform FV imaging. FV imaging was conducted under high ionic strength (HIS) buffer (10 mM HEPES, 150 mM NaCl, pH 7.0) and low ionic strength (LIS) buffer (10 mM HEPES, 1 mM NaCl, pH 7.0) at room temperature (RT). FV images (32 × 32 force curves) were collected at a scan rate of 0.07 Hz in relative trigger mode (63).

RESULTS

FV images can selectively show the force spectra when the probe is moved toward the surface (approach direction) or withdrawn from it (retract direction). Along the force curves (either approach or retract), a z-displacement position is selected and the force at this displacement for each pixel in the image is used to create a force map. In approach FV images, a bright pixel means an increase in repulsive force. In contrast, in retract FV images, a dark pixel indicates an increase in adhesive force.

To probe the role of CHOL in the mechanics of lipid microdomains, we prepared SLBs of sphingomyelin (SM), SM/CHOL (3:1, mol/mol), DOPC/dioleoylphosphatidylserine (DOPS) (1:1, mol/mol), DOPC/DOPS/CHOL (45:45:10, mol/mol/mol) on mica. Additionally, DOPC/DOPS/SM (1:1:2, mol/mol/mol) SLBs were prepared with increasing amounts

of CHOL (varied from 0 to 50 mol % of the total amount of lipid). Each sample was imaged initially by tapping-mode AFM in fluid, followed by contact-mode imaging in fluid when simultaneous FV images were collected. Initial experiments using SM and DOPC/DOPS (1:1, mol/mol) SLBs facilitated the identification of SM-rich domains and determination of force and trigger set points required to image more complex bilayers. As previously reported, the formation of SLBs on mica is governed by electrostatic interactions due to variation in the headgroup charge in different ionic strength buffers (64). This variation in the headgroup charge, and hence the lipid-lipid interaction, will affect the AFM tip-bilayer interactions and thus the breakthrough for bilayers will vary with ionic strength. FV imaging of SLBs was conducted under HIS and LIS conditions to map the breakthrough forces during approach and the adhesion during retraction of the AFM tip.

SM and SM/CHOL (3:1, mol/mol) SLB

In the absence of CHOL, the SM bilayer showed compact and planar structures under HIS buffer (pH 7.0) at RT (Fig. 1 *a*). Some bare mica areas were visible and double bilayers were formed during vesicle fusion. Using defects in the single bilayer and cross-section analysis, we determined the thickness of the SM bilayers (Fig. 1 *b*) to be 6.1 nm ± 0.2 nm ($n = 50$), and the thickness of the double bilayers was approximately double that. Fig. 1 *b* illustrates a typical force curve on an SM bilayer under HIS buffer. A discontinuity was observed in the contact region of the approach curve, indicating a sudden movement of the tip toward to the surface. The force at which this event occurs corresponds to the breakthrough force of the bilayer. The measured breakthrough forces under both HIS and LIS buffer are shown in Fig. 1, *c* and *d*. The breakthrough force under LIS buffer (0.78 nN, Gaussian width (GW) = 0.04 nN) was much smaller than that under HIS buffer (6.60 nN, GW = 0.50 nN) (Table S1).

The mixture of SM/CHOL (3:1, mol/mol) exhibited a bilayer with an apparent height of 5.2 nm ± 0.3 nm, as measured again using bare patches (Fig. 1 *e*). The bilayer surface also showed some wrinkle-like features. These features likely reflect an incomplete packing of the lipids in

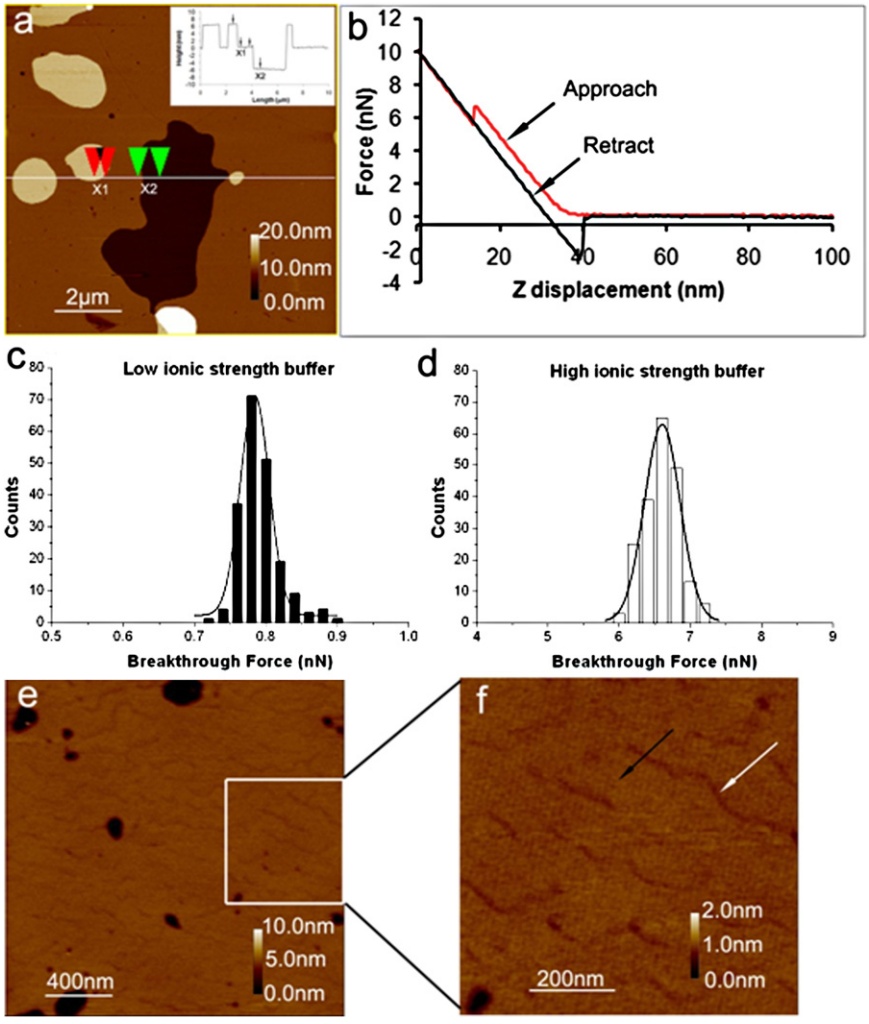

FIGURE 1 Visualization and force measurement of SM and SM/CHOL (3:1, mol/mol) bilayers. (*a*) AFM height image of SM bilayer; scan size: 10 × 10 μm^2; height scale: 20 nm. The inset image is a cross section of the line in *a*, showing bilayer thickness at position X1 or X2 was ~6.1 nm. (*b*) Force spectroscopy on SM bilayers, showing a discontinuity corresponding to the force required to puncture the SM bilayers. Breakthrough forces of SM bilayers under LIS (*c*) and HIS (*d*) solutions. Lines are fits of the histograms to Gaussian distributions. (*e*) AFM height image of SM/CHOL (3:1, mol/mol) bilayers showed the heterogeneity of membrane. Scan size: 2 × 2 μm^2; height scale: 10 nm. (*f*) Zoom of the region in *e* showing LD structures (*white arrow*) that are 0.2 nm lower than the main domain. Scan size: 800 × 800 nm^2; height scale: 2 nm.

the bilayer due to the intersection of two spreading vesicles. Similar processes give rise to crystal defects when two crystal faces grow into one another. This interpretation is supported by the apparent height difference of 0.2 ± 0.04 nm (Fig. 1 *f*) between the main bilayer regions and the regions of looser packing. The areas with lower packing density are lower, as expected. Under HIS conditions, the breakthrough force of the SM/CHOL (3:1, mol/mol) bilayer was distributed around 6.21 nN (GW = 0.84 nN) in the main (HD) bilayer regions (marked by the *black arrow* in Fig. 1 *f*) and 4.28 nN (GW = 0.57 nN) in the lower domains (LDs; marked by the *white arrow* in Fig. 1 *f*), again supporting the incomplete packing theory for the LDs. AFM imaging experiments in LIS buffer for this system proved very difficult due to tip contamination.

DOPC/DOPS (1:1, mol/mol) and DOPC/DOPS/CHOL (45:45:10, mol/mol/mol)

A binary bilayer of DOPC and DOPS was prepared at a mole ratio of 1:1. No phase separation was observed for the binary SLBs (Fig. 2 *a*), since both DOPC and DOPS have the same unsaturated hydrocarbon chains, and the phase transition temperatures are below 0°C (DOPC −15°C; DOPS −11°C, according to the supplier (65)). At RT, the DOPC/DOPS bilayer exists in a liquid-crystalline phase. The thickness of this binary bilayer was 4.1 ± 0.1 nm, as measured using defects in the bilayer. The breakthrough force was 4.38 nN (GW = 0.51 nN) under HIS conditions and 3.58 nN (GW = 0.64 nN) in LIS buffer.

FV imaging was done on DOPC/DOPS (1:1, mol/mol) bilayers containing 10 mol % CHOL. Fig. 2 *b* shows the topography

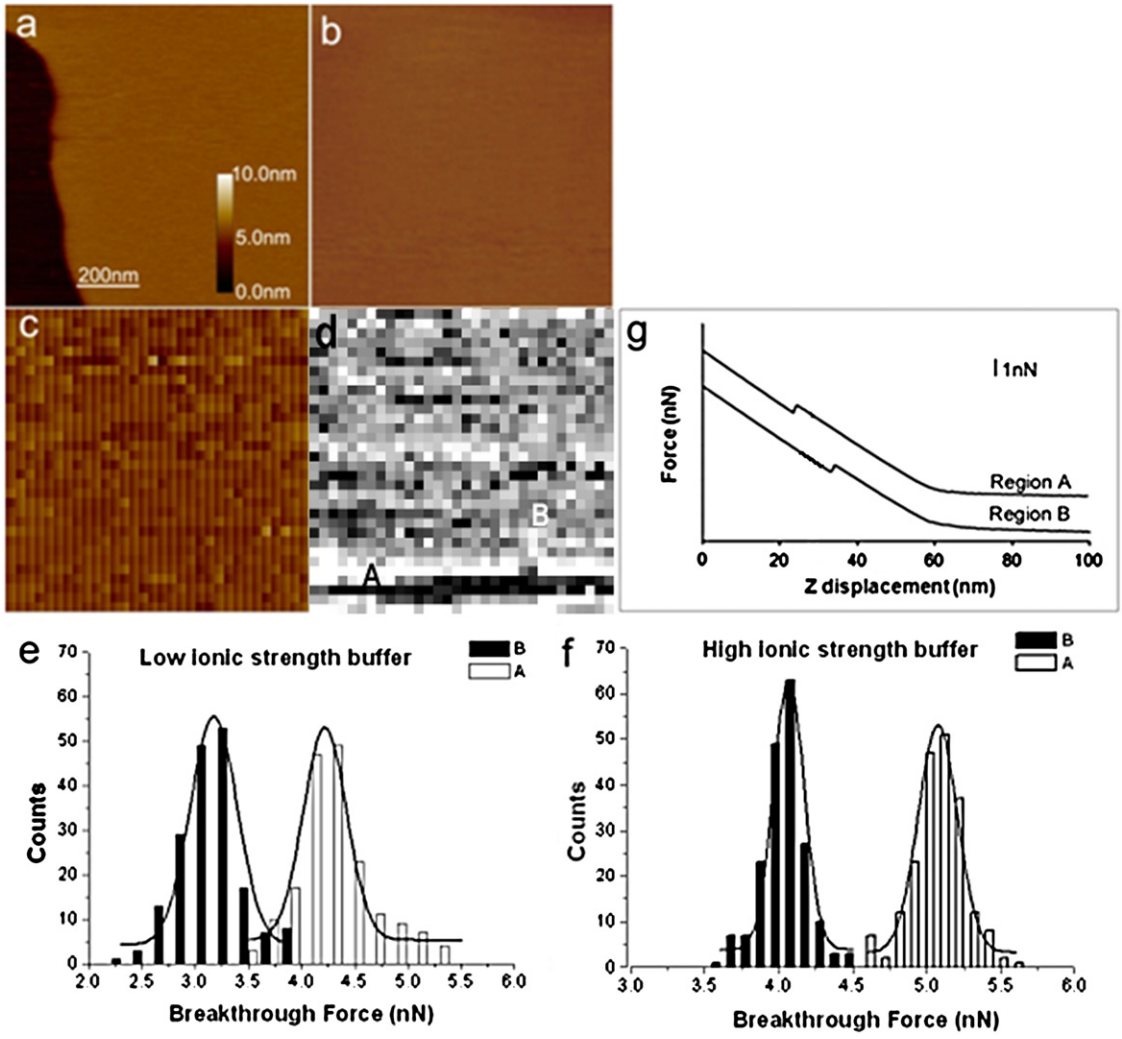

FIGURE 2 Observation and force analysis on DOPC/DOPS (1:1, mol/mol) and DOPC/DOPS/CHOL (45:45:10, mol/mol/mol). (*a*) Typical AFM height image of the DOPC/DOPS (1:1, mol/mol) bilayer. (*b*) AFM height image of the DOPC/DOPS/CHOL (45:45:10, mol/mol/mol) bilayer. (*c*) Topography image in FV mode of the bilayer in *b*. (*d*) Breakthrough map created using approach-force curves such as those shown in *g*. (*a–d*) Scan size: 1 μm × 1 μm. (*a–c*) Height scale: 10 nm. (*d*) Force scale: 3.0 nN. Breakthrough force distribution in regions A and B under LIS (*e*) and HIS (*f*) ($n \approx 200$ for both distributions). Lines are fits of the histograms to Gaussian distributions. (*g*) Typical approach-force curves observed in the areas labeled in *d*.

of the DOPC/DOPS/CHOL (45:45:10, mol/mol/mol) bilayer imaged at high resolution (512 × 512 points). The height image (Fig. 2 *c*) collected in FV mode (lower resolution) was similar to Fig. 2 *b*. There was no significant difference in topography with and without CHOL (compare Fig. 2, *a* and *b*). However, the FV image obtained under HIS solution using the approach-force curves showed considerable contrast (Fig. 2 *d*). The FV image highlighted that two different breakthrough forces are observed corresponding to the two force curves shown in Fig. 2 *g*. The distributions of breakthrough forces for the DOPC/DOPS/CHOL (45:45:10, mol/mol/mol) bilayers are depicted in Fig. 2, *e* and *f*, under LIS and HIS conditions, respectively. For Fig. 2, *e* and *f*, ~200 forces curves from each region were used to obtain the distributions to allow easy comparison. In HIS buffer, the average breakthrough force in region A of Fig. 2 *d* was significantly higher (5.07 nN, GW = 0.27 nN) than that in region B, (4.07 nN, GW = 0.21 nN). Similarly, under LIS conditions, the average breakthrough force in region A was again higher (4.22 nN, GW = 0.41 nN) than that in region B (3.17 nN, GW = 0.44 nN). In both cases, the breakthrough forces in region B were similar to that for CHOL-free DOPC/DOPS (1:1, mol/mol) bilayers (Table S1). The area of higher breakthrough force in Fig. 2 *d* (labeled A) accounts for almost 10% of the image area, suggesting that these areas of the bilayer are CHOL-rich. Similar domains have been observed using fluorescence imaging of DOPC/DOPS bilayers (66).

DOPC/DOPS/SM (1:1:2, mol/mol/mol)

Without CHOL, DOPC/DOPS/SM (1:1:2) bilayers at RT are expected to have both a liquid-crystalline phase and a gel phase because SM has a phase transition temperature of 40°C (67). Therefore, at RT only the component containing SM exists in the gel state, and these SM-rich sections are observed as an HD with a height of 5.6 nm similar to the SM bilayer thickness (Fig. 1 *a*). These gel domains within a softer, more fluid bilayer are often termed microdomains. There are many circumstances, such as protein or CHOL inclusion, that have been observed to give rise to micro domains (68). When CHOL was introduced, it imposed a conformational ordering upon a neighboring aliphatic chain due to its flat and rigid molecular structure. The SM gel phase and neighboring phospholipid liquid phase converted to an intermediate state, and physical properties such as thickness, fluidity, and rigidity change in turn (8). As shown in Fig. S1, DOPC/DOPS/SM bilayers exhibited phase separation such that the SM-rich domains (HD) were typically ~1.3 nm higher than the neighboring phospholipid-rich domains (LD), in agreement with previous results obtained by AFM on DOPC/SM SLBs (69). With increasing CHOL content, the difference in height between HD and LD decreased from 1.3 nm to 0.6 nm due to an increase in LD thickness from 4.2 nm to 4.8 nm (Fig. S1 *b*). However, the measured thickness of HD did not change much (e.g., , 5.5 ± 0.2 nm for the mixture without CHOL and 5.4 ± 0.2 nm for the mixture with 50 mol % CHOL).

We also performed FV imaging after zooming into a smaller region of the bilayer (Fig. 3 *a*). Fig. 3 *b* shows a topographic image of a DOPC/DOPS/SM (1:1:2, mol/mol/mol) bilayer under HIS conditions, acquired with 32 × 32 pixel resolution (Fig. 3 *b*) as opposed to 512 × 512 pixel resolution (Fig. 3 *a*). As expected, the breakthrough force on SM bilayer was larger than that on a DOPC/DOPS (1:1, mol/mol) bilayer. When the trigger value was precisely adjusted to be lower than the breakthrough force of SM-rich domains and higher than that of the phospholipid-rich domains, the different bilayer domains yielded different force curves, as shown in the FV images of the DOPC/DOPS/SM (1:1:2, mol/mol/mol) bilayer (Fig. 3, *c* and *d*). Fig. 3 *c* shows a map of breakthrough forces obtained from approach-force curves, and Fig. 3 *d* shows the adhesion map obtained from retract-force curves. Both the repulsive- and adhesive-force maps discriminate between the domains observed in the height image (Fig. 3 *b*) based on the nanomechanical response.

Fig. 3 *e* illustrates the approach-force curves for HD, LD, and the domain boundaries, respectively. In Fig. 3 *a*, these force curves show different behaviors for different domains. For example, there was no breakthrough event in HD, indicating that the load is not big enough to puncture the SM-rich domain, as expected. Discontinuities in the force curves for the LD and the domain boundaries in Fig. 3 *e* indicated that the phospholipid-rich domain and the boundary of domains are easy to puncture under the same load.

We analyzed the adhesion of different domains using the retract-force curves obtained with the trigger value lower than the breakthrough force of SM-rich domains and higher than that of the phospholipid-rich domains. The retract-force curve in an SM-rich domain (HD) did not show an adhesion. On the other hand, the retract-force curve for the phospholipid-rich domain (LD) showed an adhesion, but only when the approach trigger value was set above the breakthrough force, so that the AFM tip penetrated the bilayer and was exposed to the underlying mica. Fig. 3 *d* maps the adhesive force of the entire bilayer, showing that the adhesion force on the HD was much lower than that on the LD.

The domain boundaries are apparent in FV images as pixels of different intensity (Fig. 3, *c* and *d*). Typical domain-boundary force curves are plotted in Fig. 3, *e* and *f*. FV images under LIS conditions were also examined and showed results similar to Fig. 3 (data not shown).

The breakthrough forces on mixed bilayers with increasing CHOL content were analyzed. For DOPC/DOPS/SM (1:1:2, mol/mol/mol), FV imaging of bilayers containing 10 mol % CHOL was performed with both high and low trigger values. With a small trigger value, the tip did not puncture the HD. As shown in Fig. 4, the FV images present good phase separation corresponding to the topographic image. Force spectra in HD, LD, and the domain

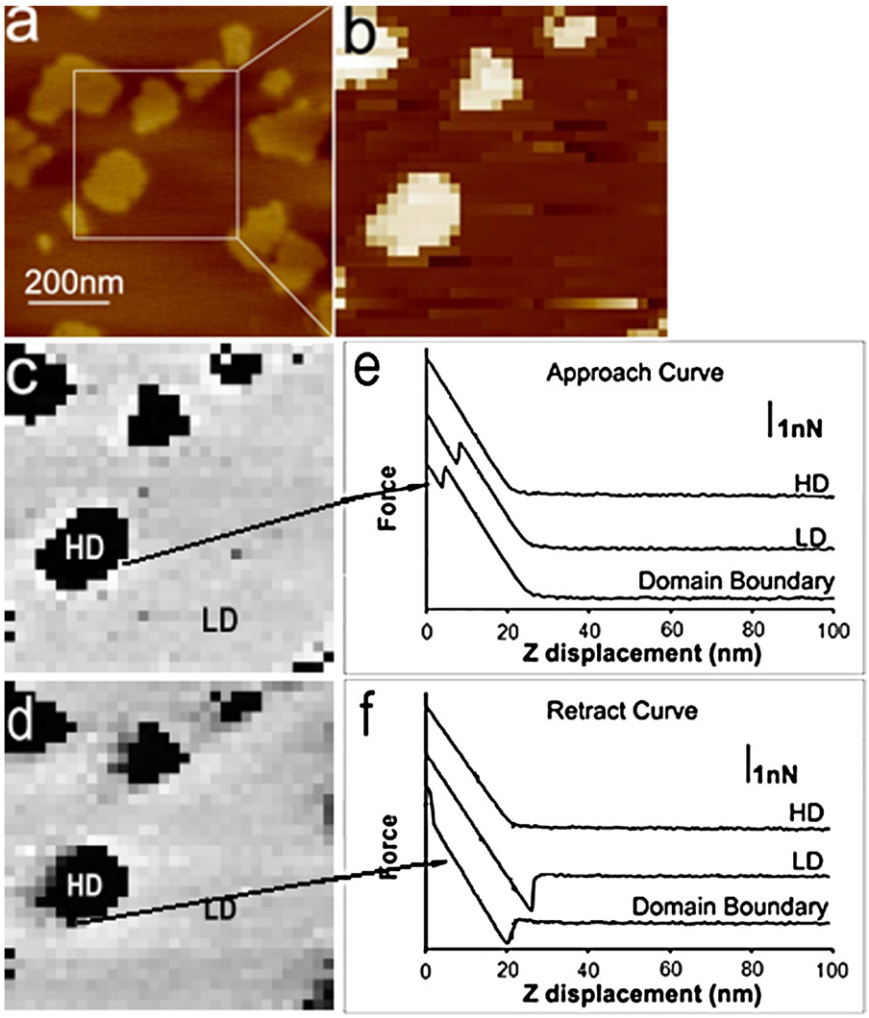

FIGURE 3 FV imaging on DOPC/DOPS/SM (1:1:2, mol/mol/mol) bilayers under HIS solutions. (*a*) AFM height image. Scan size: 1 μm $\times$ 1 μm, height scale: 5 nm, 512 $\times$ 512. (*b*) AFM height image zoomed in the area in *a*. Scan size: 500 $\times$ 500 nm^2; height scale: 5 nm, 32 $\times$ 32. (*c*) Breakthrough map created using approach-force curves such as those shown in *e*; force scale: 4.5 nN. (*d*) Adhesion map created retract-force curves such as those shown in *f*; force scale: 2.5 nN. Force curves are shown in *e* and *f*, indicating different force behavior for different domains.

boundaries shown in Fig. 4, *d* and *e*, were similar to those of the DOPC/DOPS/SM (1:1:2, mol/mol/mol) bilayers without CHOL. However, a higher average breakthrough force of ~4 nN was determined for the LD in Fig. 4 *b* compared to ~3 nN for the LD in Fig. 3 *c*. When the trigger value was increased to a force higher than the HD breakthrough force (Fig. S2), the contrast between domains in the height image was blurred, whereas phase separation in the breakthrough map (Fig. S2 *b*) was quite clear. Approach-force curves for the HD and LD are shown in Fig. S2 *c*. Both force curves show breakthrough events during approach to the SLBs. However, for the retract-force curves, no large differences as a function of lateral position on the sample were observed, indicating that adhesion for both domains was similar.

When the CHOL content was increased to 50 mol %, the AFM probe was easily contaminated and became sticky. Under such conditions, FV imaging could not be performed due to tip contamination in contact mode, even though the domains could be observed by tapping-mode AFM. For SLBs with increasing CHOL content from 0 to 33 mol %, the breakthrough forces on HD and LD were analyzed (Table S1, Fig. S3). The breakthrough forces on HD under HIS conditions showed a decreasing trend from 6.77 nN (GW = 0.58 nN) to 4.46 nN (GW = 0.53 nN) upon increasing CHOL content from 0 to 33 mol %. In contrast, the observed breakthrough force on LD in HIS buffer did not show a clear trend. Nevertheless, the LD breakthrough forces under HIS conditions were always lower than the HD forces (Table S1).

Under LIS conditions, the observed breakthrough forces increased for both HD and LD with increasing CHOL content. The HD and LD breakthrough forces increased ~30% and ~200%, respectively, when CHOL content increased from 0 to 33 mol %.

Force curves at lipid domain boundaries

During FV imaging, normal approach-force curves showed a discontinuity when the load was high enough to puncture the SLBs (Fig. 4 *d* and Fig. S2 *c*), and no discontinuity

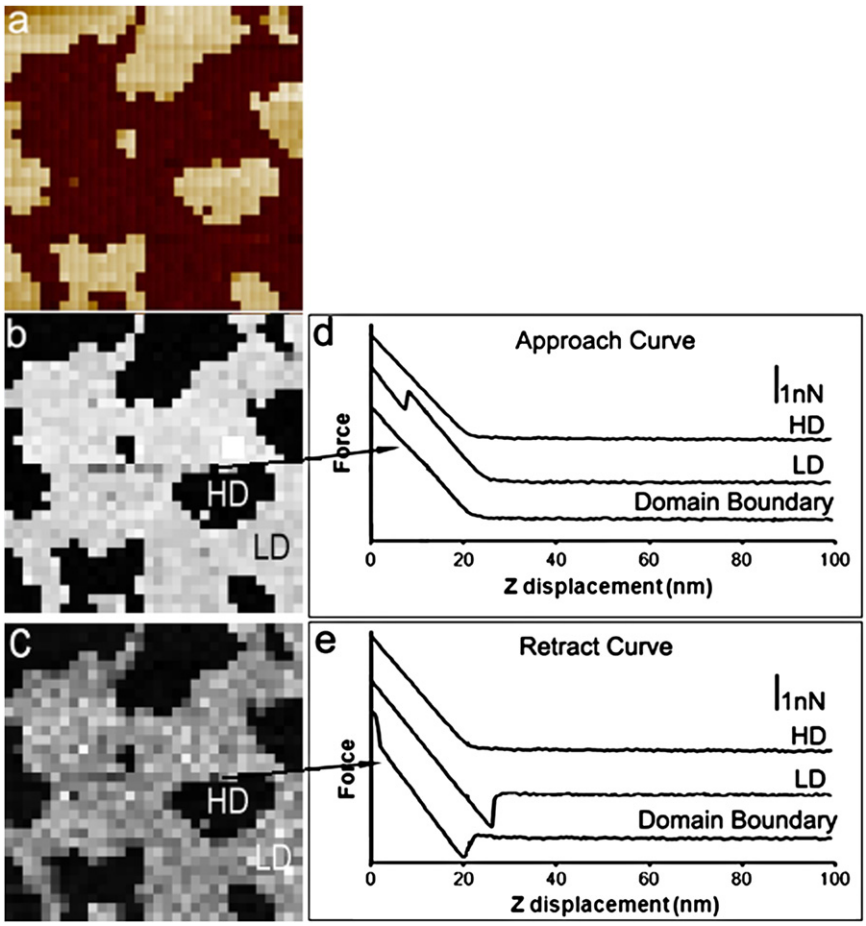

FIGURE 4 FV images at a trigger value of 4.8 nN on DOPC/DOPS/SM (1:1:2, mol/mol/mol) bilayers containing 10 mol % CHOL under HIS conditions. (*a*) AFM height image. Scan size: 500 × 500 nm^2; height scale: 5 nm. (*b*) Breakthrough map created using approach-force curves such as those shown in *d*; force scale: 4.0 nN. (*c*) Adhesion map created retract-force curves such as those shown in *e*; force scale: 1.5 nN. Force spectra of lighter regions in the repulsive-force map (*b*) correspond to lower force associated with the LD, and those of black regions in *b* correspond to the HD shown in *a*. The black regions in the adhesion map (*arrow* in *c*) show induced order regions.

otherwise (HD in Figs. 3 *e* and 4 *d*). This was true for most parts of the mixed bilayers. However, on the boundary of HD and LD, an unusual force curve was observed when the trigger was set to a value slightly lower than the threshold force to breakthrough HD. As shown in Figs. 3 *f* and 4 *e*, there were no discontinuities observed on the approach curve. However, when the probe was retracted, a discontinuity was observed at the start of the retract cycle. To the best of our knowledge, such force behavior has not been observed previously on phospholipid bilayers.

Adhesion on mixed bilayers

FV imaging also allowed us to analyze adhesion. The effect of CHOL on membrane cytoskeleton adhesion is considered an important factor in cellular mechanical properties (70). To assess the adhesion, we had to set the trigger to be smaller than the threshold force to break through the bilayers (Fig. 4 *d*). If the probe breaks through the bilayers (see for example Fig. 4 *e*), the adhesion could due to interactions between the probe and the solid support rather than probe-bilayer interactions. No adhesion was found under HIS or LIS conditions for trigger values below the breakthrough force in any of the samples.

DISCUSSION

Elucidating CHOL's role in the formation and maintenance of more highly ordered membrane domains has been of significant interest for some time. Exactly how CHOL helps membrane domains mediate stress-induced mechanotransduction is still not fully understood. In this work, microdomains were observed as higher regions in the bilayers containing SM and were still present after addition of CHOL. Using FV imaging, we demonstrated the ability to sense mechanical properties as a function of lateral phase separation with a high resolution on the scale of 10–20 nm. Our goal was to investigate the effect of CHOL on the rigidity of the cellular membrane. SLBs of SM, phospholipids, and mixtures of SM and phospholipids were used as model membranes.

The initial aim of these experiments was to elucidate membrane properties in the absence of CHOL. We used two different buffer systems in which the HIS buffer was similar to the physiological environment of mammalian cells. The mechanical properties under HIS conditions mimic the real situation in which the cellular membrane responds to mechanical pressure and thus mediated mechanotransduction (17,18,71). Although LIS conditions may not have a direct relation to the physiological situation, changes in

the strength of the interactions between headgroups can help elucidate the important forces governing the material properties of the bilayer.

A study by imaging mass spectrometry shows that there is significant intermixing of components in phase-separated lipid structures. For example, SM-rich domains are not exclusively composed of SM, and phospholipid-rich domains contain other components (72). It is reasonable to assume that domains formed in multicomponent systems would have different physical properties compared to pure bilayers of the same nominal composition, given the presence of small amounts of other species. For example, the height of SM-rich domains (without CHOL) in the DOPC/DOPS/SM bilayers was ~0.5 nm lower than that of pure SM bilayers.

Differences in repulsive or adhesive force could also be seen at domain boundaries in DOPC/DOPS/SM (1:1:2, mol/mol/mol) bilayers. For HIS solutions, breakthrough forces at the boundary regions were somewhere between those for HD and LD, indicating a different structure or a transition region. This interpretation was strengthened by the observation of force curves with discontinuities in the retract traces (Fig. 3 *f*) in the boundary regions.

Some force curves observed at the domain boundaries (Figs. 3 *f* and 4 *e*) suggest that when it starts to retract from the surface, the tip is suddenly subjected to much stronger forces. We speculate that this is due to an ordering of the edge of the HD as the tip pushes past it into the LD. Although the HD is more ordered than the LD, at the edge there must be some disorder due to incomplete two-dimensional packing. During approach, the tip induces better packing along the edge. When the tip is then retracted, it experiences the briefly increased stiffness of the more-ordered HD until it reaches a critical point where the order is lost and the stiffness decreases. These force curves were observed exclusively at the boundary of SM-rich domains. We should point out that we cannot discount the possibility that the unusual force curves may also be a result of the interaction geometry between the tip and surface over which we have no direct control.

With respect to the complexity of the headgroup structures, hydrocarbon chain length, and the degree of unsaturation of the acyl chains, it is difficult to predict the physical properties of individual lipids interacting with CHOL. The insertion of CHOL into the planar bilayers will lead to a laterally condensed membrane (73,74). The addition of 25 mol % CHOL leads to the appearance of domains that are slightly thinner than pure SM bilayers. These domains are likely areas of poorer lipid packing and may result from a higher local level of CHOL that interrupts the SM packing. The area of the LDs accounts for only 9% of the total image area, which indicates that although there may be areas of higher CHOL concentration, much of the CHOL is spread throughout the SM/CHOL (3:1, mol/mol) bilayer. Under HIS conditions, the breakthrough forces of the mixture of SM/CHOL (3:1, mol/mol) bilayers presented two distributions centered at 6.21 nN and 4.28 nN. The breakthrough force on the LDs (4.28 nN) was considerably lower than that of pure SM bilayers (6.60 nN). These lower breakthrough forces suggest a looser packing in these domains.

The presence of localized areas of higher CHOL concentration is also observed in the phospholipid (DOPC/DOPS) bilayer. Although not much height difference was observed in DOPC/DOPS (1:1, mol/mol) bilayers with 10 mol % CHOL, heterogeneities in the breakthrough force map were observed (see Fig. 2 *d*). In contrast to the SM case, CHOL in the DOPC/DOPS layer increases the breakthrough forces. These results are not surprising since CHOL in a loosely packed liquid-crystalline layer such as DOPC/DOPS would likely help stabilize intermolecular interactions between lipids, increasing rigidity, whereas CHOL would likely interrupt these interactions in a tightly packed SM bilayer, thus decreasing rigidity.

CHOL has been reported to thicken the phospholipid bilayers in the liquid phase (75,76). Our AFM work agrees with previous findings that CHOL increases the thickness of phospholipid-rich domains. The situation is rather different for SM bilayers. An x-ray study by Maulik and Shipley (77) showed that the thickness of the bilayers of C18:0-SM decreased from 5.2 nm to 4.6 nm with the addition of 50 mol % CHOL. The SM we used in our work was C17:0-SM, which is similar to C18:0-SM in that it is composed of hydrocarbon acyl chains, and the thickness of the pure SM bilayer decreased from 6.1 nm to 5.2 nm upon addition of 25 mol % CHOL. However, as shown in Fig. S1 *b*, the thickness of SM-rich domains in DOPC/DOPS/SM (1:1:2) bilayers did not change with CHOL concentration. We suggest that this is due to residual amounts of DOPC and DOPS mixed in with the SM component. As discussed earlier, CHOL has opposite effects on the thickness of the SM (decreasing effect) and DOPC/DOPC (increasing effect). These two effects may partially balance each other, and hence no change in thickness will be observed for the SM-rich domains in DOPC/DOPS/SM.

In the case of mixed bilayers, lipid microdomains are probably formed driven by lipid-lipid interactions (8). Lipids with fully saturated acyl chains and the same headgroups tend to be the most miscible (78). SM is composed of long, saturated fatty acyl chains that can pack tightly, and therefore has a high propensity to form domains in a phospholipid matrix even without CHOL. CHOL has been shown to interact preferentially with SM in a mixed lipid bilayer (79). In contrast to phospholipids, SM possesses both hydrogen bond-acceptor and donor groups. The hydrogen bonding is believed to contribute to CHOL-SM interactions. Additionally, the amide linkage in SM molecules has been reported to be important for interactions with CHOL (80,81).

In this study, the domain mechanical properties in the mixed bilayer changed with varying CHOL concentrations. In a study using pure SM bilayers, Li et al. (82) found that

SM-CHOL interactions decreased the in-plane elasticity of a pure SM monolayer, demonstrating the effect of CHOL on bilayer mechanical properties. Rigidity changes can be qualitatively explained by variation in the threshold force to breakthrough bilayers before and after CHOL addition. CHOL incorporation leads to phase transition of the lipid membrane from a solid-ordered to a liquid-ordered phase, or from a liquid-disordered to a liquid-ordered phase (19). For HIS, increasing CHOL lowers the rigidity of the HD, as expected. Therefore, CHOL softens the SM-rich domains. Of interest, the breakthrough force of HD appears to change slowly below 20 mol % (see Table S1), indicating that the mechanical properties of SM-rich domains do not change rapidly with the addition of small amounts of CHOL. This could be due to the strength of the headgroup interactions, which are strong enough to either prevent the initial incorporation of CHOL or (more likely) maintain the SM-rich domain structure even with small amounts of CHOL present. The breakthrough force of the LD remains unchanged at HIS. The liquid nature of the LD bilayer interior may be fluid enough to accommodate the CHOL without changing the headgroup structure, and consequently keep the breakthrough force relatively constant.

It is interesting to note that the presence of CHOL dramatically reduces the likelihood of induced packing at the domain boundaries. The presence of CHOL in the SM-rich domain may mean an even greater disorder at the boundary, and the approach of the tip does not cause enough of a rearrangement to overcome the extra disorder.

CONCLUSIONS

In this work, we studied the effects of CHOL on the mechanical properties of SLBs by means of FV imaging. The diameter of the AFM tips used in this study was ~15 nm, and therefore our technique is sensitive to lateral lipid composition on the scale of 10–20 nm. Because of the lateral heterogeneity of bilayers, different regions of the bilayers respond differently to an applied force, and this response can be examined in detail by FV imaging. This work provides substantial evidence of the dynamic rigidity of the different phase domains as a function of the amount of CHOL in the system. We have for the first time observed mechanical induction of order at domain boundaries. Our results indicate that the mechanical response of the cellular membrane may be modulated by CHOL organization in a physiological environment.

SUPPORTING MATERIAL

Methods, three figures, and one table are available at http://www.biophysj.org/biophysj/supplemental/S0006-3495(10)00622-3.

This work was supported by the Australian Microscopy and Microanalysis Research Facility and the Australian Research Council.

REFERENCES

1. Pike, L. J. 2006. Rafts defined: a report on the Keystone Symposium on Lipid Rafts and Cell Function. *J. Lipid Res.* 47:1597–1598.
2. Lagerholm, B. C., G. E. Weinreb, …, N. L. Thompson. 2005. Detecting microdomains in intact cell membranes. *Annu. Rev. Phys. Chem.* 56:309–336.
3. Silvius, J. 2005. Lipid microdomains in model and biological membranes: how strong are the connections? *Q. Rev. Biophys.* 38:373–383.
4. Simons, K., and D. Toomre. 2000. Lipid rafts and signal transduction. *Nat. Rev. Mol. Cell Biol.* 1:31–39.
5. Simons, K., and E. Ikonen. 1997. Functional rafts in cell membranes. *Nature.* 387:569–572.
6. Lingwood, D., and K. Simons. 2009. Lipid rafts as a membrane-organizing principle. *Science.* 327:46–50.
7. Nielsen, M., J. Thewalt, …, O. G. Mouritsen. 2000. Sterol evolution and the physics of membranes. *Europhys. Lett.* 52:368–374.
8. Ohvo-Rekilä, H., B. Ramstedt, …, J. Peter Slotte. 2002. Cholesterol interactions with phospholipids in membranes. *Prog. Lipid Res.* 41:66–97.
9. Haines, T. H. 2001. Do sterols reduce proton and sodium leaks through lipid bilayers? *Prog. Lipid Res.* 40:299–324.
10. Incardona, J. P., and S. Eaton. 2000. Cholesterol in signal transduction. *Curr. Opin. Cell Biol.* 12:193–203.
11. Brown, D. A., and E. London. 1998. Functions of lipid rafts in biological membranes. *Annu. Rev. Cell Dev. Biol.* 14:111–136.
12. Pediconi, M. F., C. E. Gallegos, …, F. J. Barrantes. 2004. Metabolic cholesterol depletion hinders cell-surface trafficking of the nicotinic acetylcholine receptor. *Neuroscience.* 128:239–249.
13. Pol, A., S. Martin, …, R. G. Parton. 2005. Cholesterol and fatty acids regulate dynamic caveolin trafficking through the Golgi complex and between the cell surface and lipid bodies. *Mol. Biol. Cell.* 16: 2091–2105.
14. Ikonen, E. 2001. Roles of lipid rafts in membrane transport. *Curr. Opin. Cell Biol.* 13:470–477.
15. Saher, G., B. Brügger, …, K.-A. Nave. 2005. High cholesterol level is essential for myelin membrane growth. *Nat. Neurosci.* 8:468–475.
16. Shadan, S., P. S. James, …, R. Jones. 2004. Cholesterol efflux alters lipid raft stability and distribution during capacitation of boar spermatozoa. *Biol. Reprod.* 71:253–265.
17. Park, H., Y.-M. Go, …, H. Jo. 1998. Plasma membrane cholesterol is a key molecule in shear stress-dependent activation of extracellular signal-regulated kinase. *J. Biol. Chem.* 273:32304–32311.
18. Ferraro, J. T., M. Daneshmand, …, V. Rizzo. 2004. Depletion of plasma membrane cholesterol dampens hydrostatic pressure and shear stress-induced mechanotransduction pathways in osteoblast cultures. *Am. J. Physiol. Cell Physiol.* 286:C831–C839.
19. McMullen, T. P. W., R. N. A. H. Lewis, and R. N. McElhaney. 2004. Cholesterol-phospholipid interactions, the liquid-ordered phase and lipid rafts in model and biological membranes. *Curr. Opin. Colloid Interface Sci.* 8:459–468.
20. Korade, Z., and A. K. Kenworthy. 2008. Lipid rafts, cholesterol, and the brain. *Neuropharmacology.* 55:1265–1273.
21. Reviakine, I., and A. Brisson. 2000. Formation of supported phospholipid bilayers from unilamellar vesicles investigated by atomic force microscopy. *Langmuir.* 16:1806–1815.
22. Kraft, M. L., P. K. Weber, …, S. G. Boxer. 2006. Phase separation of lipid membranes analyzed with high-resolution secondary ion mass spectrometry. *Science.* 313:1948–1951.
23. Burns, A. R., D. J. Frankel, and T. Buranda. 2005. Local mobility in lipid domains of supported bilayers characterized by atomic force microscopy and fluorescence correlation spectroscopy. *Biophys. J.* 89:1081–1093.

24. Domenech, O., A. Morros, …, J. Hernandez-Borrell. 2007. Supported planar bilayers from hexagonal phases. *Biochim. Biophys. Acta*. 1768:100–106.
25. Chiantia, S., J. Ries, …, P. Schwille. 2006. Combined AFM and two-focus SFCS study of raft-exhibiting model membranes. *ChemPhysChem*. 7:2409–2418.
26. Nussio, M. R., M. Liddell, …, J. G. Shapter. 2007. Dynamics of phospholipid membrane growth and drug-membrane interactions probed by atomic force microscopy (AFM). *J. Scan. Probe Microsc*. 2:42–46.
27. Montero, M. T., M. Pijoan, …, J. Hernandez-Borrell. 2006. Interfacial membrane effects of fluoroquinolones as revealed by a combination of fluorescence binding experiments and atomic force microscopy observations. *Langmuir*. 22:7574–7578.
28. Leonenko, Z., E. Finot, and D. Cramb. 2006. AFM study of interaction forces in supported planar DPPC bilayers in the presence of general anesthetic halothane. *Biochim. Biophys. Acta*. 1758:487–492.
29. Berquand, A., M. P. Mingeot-Leclercq, and Y. F. Dufrêne. 2004. Real-time imaging of drug-membrane interactions by atomic force microscopy. *Biochim. Biophys. Acta*. 1664:198–205.
30. Merino-Montero, S., O. Domenech, …, J. Hernandez-Borrell. 2006. Preliminary atomic force microscopy study of two-dimensional crystals of lactose permease from *Escherichia coli*. *Biophys. Chem*. 119:78–83.
31. Mueller, H., H.-J. Butt, and E. Bamberg. 2000. Adsorption of membrane-associated proteins to lipid bilayers studied with an atomic force microscope: myelin basic protein and cytochrome *c*. *J. Phys. Chem. B*. 104:4552–4559.
32. Reimhult, E., F. Hook, and B. Kasemo. 2003. Intact vesicle adsorption and supported biomembrane formation from vesicles in solution: influence of surface chemistry, vesicle size, temperature, and osmotic pressure. *Langmuir*. 19:1681–1691.
33. Sackmann, E. 1996. Supported membranes: scientific and practical applications. *Science*. 271:43–48.
34. Nussio, M. R., M. J. Sykes, …, J. G. Shapter. 2009. Kinetics membrane disruption due to drug interactions of chlorpromazine hydrochloride. *Langmuir*. 25:1086–1090.
35. Milhiet, P.-E., M.-C. Giocondi, …, C. L. Grimellec. 2002. Spontaneous insertion and partitioning of alkaline phosphatase into model lipid rafts. *EMBO Rep*. 3:485–490.
36. Feigenson, G. W. 2006. Phase behavior of lipid mixtures. *Nat. Chem. Biol*. 2:560–563.
37. Baumgart, T., S. T. Hess, and W. W. Webb. 2003. Imaging coexisting fluid domains in biomembrane models coupling curvature and line tension. *Nature*. 425:821–824.
38. Veatch, S. L., and S. L. . Keller. 2005. Miscibility phase diagrams of giant vesicles containing sphingomyelin. *Phys. Rev. Lett*. 94:148101.
39. Gaus, K., E. Gratton, …, W. Jessup. 2003. Visualizing lipid structure and raft domains in living cells with two-photon microscopy. *Proc. Natl. Acad. Sci. USA*. 100:15554–15559.
40. Parasassi, T., and E. Gratton. 1995. Membrane lipid domains and dynamics as detected by Laurdan fluorescence. *J. Fluoresc*. 5:59–69.
41. Harris, F. M., K. B. Best, and J. D. Bell. 2002. Use of Laurdan fluorescence intensity and polarization to distinguish between changes in membrane fluidity and phospholipid order. *Biochim. Biophys. Acta*. 1565:123–128.
42. Kusube, M., N. Tamai, …, S. Kaneshina. 2005. Pressure-induced phase transitions of lipid bilayers observed by fluorescent probes Prodan and Laurdan. *Biophys. Chem*. 117:199–206.
43. Lentz, B. R. 1989. Membrane ''fluidity'' as detected by diphenylhexatriene probes. *Chem. Phys. Lipids*. 50:171–190.
44. Lentz, B. R. 1993. Use of fluorescent probes to monitor molecular order and motions within liposome bilayers. *Chem. Phys. Lipids*. 64:99–116.
45. Repakova, J., J. M. Holopainen, …, I. Vattulainen. 2005. Influence of DPH on the structure and dynamics of a DPPC bilayer. *Biophys. J*. 88:3398–3410.
46. Oncins, G., S. Garcia-Manyes, and F. Sanz. 2005. Study of frictional properties of a phospholipid bilayer in a liquid environment with lateral force microscopy as a function of NaCl concentration. *Langmuir*. 21:7373–7379.
47. Krüger, S., D. Krüger, and A. Janshoff. 2004. Scanning force microscopy based rapid force curve acquisition on supported lipid bilayers: experiments and simulations using pulsed force mode. *ChemPhysChem*. 5:989–997.
48. Gigler, A., C. Gnahm, …, S. Walheim. 2007. Towards quantitative materials characterization with digital pulsed force mode imaging. *J. Phys. Conf. Ser*. 61:346–351.
49. Mizes, H. A., K. G. Loh, …, E. F. Grabowski. 1991. Submicron probe of polymer adhesion with atomic force microscopy: dependence on topography and material inhomogeneities. *Appl. Phys. Lett*. 59:2901–2903.
50. Eaton, P., J. R. Smith, …, J. Tsibouklis. 2002. Adhesion force mapping of polymer surfaces: factors influencing force of adhesion. *Langmuir*. 18:3387–3389.
51. Parbhu, A. N., W. G. Bryson, and R. Lal. 1999. Disulfide bonds in the outer layer of keratin fibers confer higher mechanical rigidity: correlative nano-indentation and elasticity measurement with an AFM. *Biochemistry*. 38:11755–11761.
52. Poggi, M. A., P. T. Lillehei, and L. A. Bottomley. 2005. Chemical force microscopy on the sidewalls of single walled carbon nanotubes. *Chem. Mater*. 17:4289–4295.
53. Tan, S., R. L. Sherman, and W. T. Ford. 2004. Nanoscale compression of polymer microspheres by atomic force microscopy. *Langmuir*. 20:7015–7020.
54. Song, J., J. F. L. Duval, …, G. J. Vancso. 2007. Surface ionization state and nanoscale chemical composition of UV-irradiated poly(dimethylsiloxane) probed by chemical force microscopy, force titration, and electrokinetic measurements. *Langmuir*. 23:5430–5438.
55. Quist, A. P., S. K. Rhee, …, R. Lal. 2000. Physiological role of gap-junctional hemichannels: extracellular calcium-dependent isosmotic volume regulation. *J. Cell Biol*. 148:1063–1074.
56. Reddy, C. V., K. Malinowska, …, R. Wang. 2004. Identification of TrkA on living PC12 cells by atomic force microscopy. *Biochim. Biophys. Acta*. 1667:15–25.
57. Dague, E., D. Alsteens, …, Y. F. Dufrêne. 2007. Chemical force microscopy of single live cells. *Nano Lett*. 7:3026–3030.
59. Dufrêne, Y. F., W. R. Barger, …, G. U. Lee. 1997. Nanoscale-scale surface properties of mixed phospholipid monolayers and bilayers. *Langmuir*. 13:4779–4784.
59. Dufrêne, Y. F., T. Boland, …, G. U. Lee. 1998. Characterization of the physical properties of model biomembranes at the nanometer scale with the atomic force microscope. *Faraday Discuss*. 111:79–94.
60. Schneider, J., Y. F. Dufrene, …, G. U. Lee. 2000. Atomic force microscope image contrast mechanisms on supported lipid bilayers. *Biophys. J*. 79:1107–1118.
61. Müller, D. J., and Y. F. Dufrêne. 2008. Atomic force microscopy as a multifunctional molecular toolbox in nanobiotechnology. *Nat. Nanotechnol*. 3:261–269.
62. Sullan, R. M. A., J. K. Li, and S. Zou. 2009. Direct correlation of structures and nanomechanical properties of multicomponent lipid bilayers. *Langmuir*. 25:7471–7477.
63. Nussio, M. R., N. H. Voelcker, …, J. G. Shapter. 2008. Lateral heterogeneities in supported bilayers from pure and mixed phosphatidylethanolamine demonstrating hydrogen bonding capacity. *Biointerphases*. 3:96–104.
64. Smondyrev, A. M., and M. L. Berkowitz. 1999. Structure of dipalmitoylphosphatidylcholine/cholesterol bilayer at low and high cholesterol concentrations: molecular dynamics simulation. *Biophys. J*. 77: 2075–2089.
65. Avanti Polar Lipids, Inc. http://www.avantilipids.com/. Accessed November, 2008.

66. Wan, C., V. Kiessling, and L. K. Tamm. 2008. Coupling of cholesterol-rich lipid phases in asymmetric bilayers. *Biochemistry*. 47:2190–2198.

67. Sot, J., L. A. Bagatolli, …, A. Alonso. 2006. Detergent-resistant, ceramide-enriched domains in sphingomyelin/ceramide bilayers. *Biophys. J.* 90:903–914.

68. Simons, K., and W. L. C. Vaz. 2004. Model systems, lipid rafts, and cell membranes1. *Annu. Rev. Biophys. Biomol. Struct.* 33:269–295.

69. Rinia, H. A., M. M. E. Snel, …, B. de Kruijff. 2001. Visualizing detergent resistant domains in model membranes with atomic force microscopy. *FEBS Lett.* 501:92–96.

70. Sun, M., N. Northup, …, G. Forgacs. 2007. The effect of cellular cholesterol on membrane-cytoskeleton adhesion. *J. Cell Sci.* 120:2223–2231.

71. Davies, P. F. 1995. Flow-mediated endothelial mechanotransduction. *Physiol. Rev.* 75:519–560.

72. Zheng, L., C. M. McQuaw, …, N. Winograd. 2007. Sphingomyelin/phosphatidylcholine and cholesterol interactions studied by imaging mass spectrometry. *J. Am. Chem. Soc.* 129:15730–15731.

73. Smaby, J. M., H. L. Brockman, and R. E. Brown. 1994. Cholesterol's interfacial interactions with sphingomyelins and-phosphatidylcholines: hydrocarbon chain structure determines the magnitude of condensation. *Biochemistry.* 33:9135–9142.

74. Hung, W.-C., M.-T. Lee, …, H. W. Huang. 2007. The condensing effect of cholesterol in lipid bilayers. *Biophys. J.* 92:3960–3967.

75. Nezil, F. A., and M. Bloom. 1992. Combined influence of cholesterol and synthetic amphiphillic peptides upon bilayer thickness in model membranes. *Biophys. J.* 61:1176–1183.

76. Pandit, S. A., S. Vasudevan, …, H. L. Scott. 2004. Sphingomyelin-cholesterol domains in phospholipid membranes: atomistic simulation. *Biophys. J.* 87:1092–1100.

77. Maulik, P. R., and G. G. Shipley. 1996. Interactions of N-stearoyl sphingomyelin with cholesterol and dipalmitoylphosphatidylcholine in bilayer membranes. *Biophys. J.* 70:2256–2265.

78. Lee, A. G. 1977. Lipid phase transitions and phase diagrams II. Mixtures involving lipids. *Biochim. Biophys. Acta.* 472:285–344.

79. Slotte, J. P. 1999. Sphingomyelin-cholesterol interactions in biological and model membranes. *Chem. Phys. Lipids.* 102:13–27.

80. Gronberg, L., Z. Ruan, …, J. P. Slotte. 1991. Interaction of cholesterol with synthetic sphingomyelin derivatives in mixed monolayers. *Biochemistry.* 30:10746–10754.

81. Kan, C. C., Z. S. Ruan, and R. Bittman. 1991. Interaction of cholesterol with sphingomyelin in bilayer membranes: evidence that the hydroxy group of sphingomyelin does not modulate the rate of cholesterol exchange between vesicles. *Biochemistry.* 30:7759–7766.

82. Li, X.-M., M. M. Momsen, …, R. E. Brown. 2001. Cholesterol decreases the interfacial elasticity and detergent solubility of sphingomyelins. *Biochemistry.* 40:5954–5963.